

Regression-free Blind Image Quality Assessment

Xiaoqi Wang^a, Jian Xiong^b, Hao Gao^b, and Weisi Lin^c

^aSun Yat-sen University, Shenzhen, China

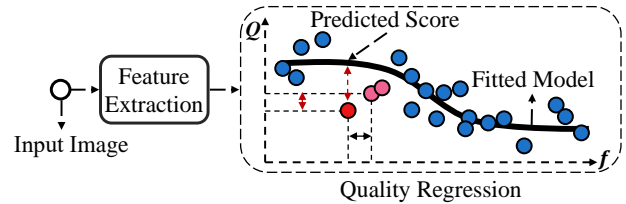
^bNanjing University of Posts and Telecommunications, Nanjing, China

^cNanyang Technological University, Singapore

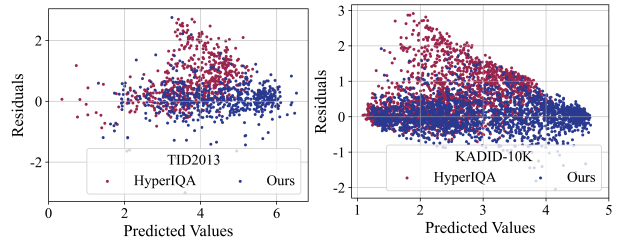
^axqwang.research@outlook.com, ^bjxiong@njupt.edu.cn, ^btsgaohao@gmail.com, ^cwslin@ntu.edu.sg

Abstract

Regression-based blind image quality assessment (IQA) models are susceptible to biased training samples, leading to a biased estimation of model parameters. To mitigate this issue, we propose a regression-free framework for image quality evaluation, which is founded upon retrieving similar instances by incorporating semantic and distortion features. The motivation behind this approach is rooted in the observation that the human visual system (HVS) has analogous visual responses to semantically similar image contents degraded by the same distortion. The proposed framework comprises two classification-based modules: semantic-based classification (SC) module and distortion-based classification (DC) module. Given a test image and an IQA database, the SC module retrieves multiple pristine images based on semantic similarity. The DC module then retrieves instances based on distortion similarity from the distorted images that correspond to each retrieved pristine image. Finally, the predicted quality score is derived by aggregating the subjective quality scores of multiple retrieved instances. Experimental results on four benchmark databases validate that the proposed model can remarkably outperform the state-of-the-art regression-based models.



(a) Regression-based BIQA model



(b) Residual plots of BIQA models

Figure 1: (a) Overview of the regression-based BIQA model. (b) Comparison of BIQA models in residual plots, where the residuals are the errors between the predicted values and the ground truth.

in the laboratory by degrading pristine images with a series of types and intensities of distortion [12, 27, 15, 10]. Then, each distorted image is evaluated by many human observers and assigned an average subjective quality score, namely mean opinion score (MOS or DMOS). A regression-based BIQA model is obtained by fitting the predicted quality scores of training images to their MOS values.

Regression-based BIQA models are composed of two main components: quality-aware feature extraction and image quality regression, as illustrated in Figure 1 (a). In traditional models [13, 23, 24, 29, 42, 46, 39, 40], researchers have utilized hand-crafted features, *e.g.*, locally normalized luminance coefficients [23], statistics of gradient, log-Gabor responses, and color statistics [46], to extract quality-aware features. Then, these features are regressed to subjective scores by a nonlinear function, *e.g.*, support vector regression (SVR) [23, 42, 13], multivariate Gaussian (MVG) model [46]. Due to the limitations of hand-

1. Introduction

Objective Image Quality Assessment (IQA) studies algorithms that automatically evaluate the visual quality of images as human judgments. It has been extensively utilized in various applications, including benchmarking visual tasks such as image restoration [28, 35], image compression [2, 20], and super resolution [14, 49], as well as for quality monitoring in various systems [44, 3]. Blind IQA (BIQA) has gained popularity in the IQA community [24, 37] over the past decade as a method for evaluating image quality without requiring reference information. In developing BIQA models, distorted images are synthesized

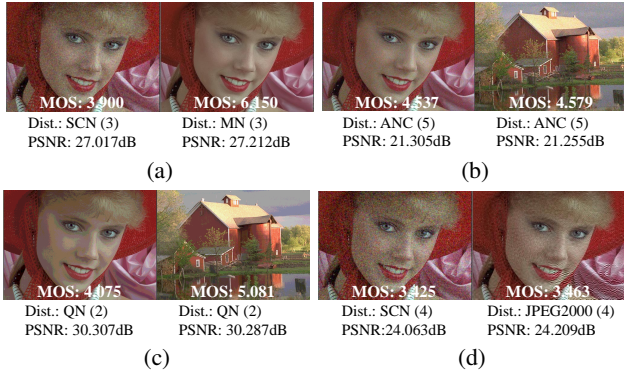


Figure 2: Illustrations of image quality scores not accurately reflecting image content and distortion. The abbreviation "Dist." stands for image distortion, including the type (and level) of distortion.

crafted features and regression functions, recent years have seen increasing use of deep learning-based BIQA models. In deep learning-based models [11, 18, 21, 48, 50, 25, 41, 32, 7], convolutional neural networks (CNN) are usually employed for extracting quality-aware features, and then the image quality score is obtained by a quality regressor, *e.g.*, multi-layer perceptron (MLP) [34, 41], hyper network [32], Transformer encoder [7, 43]. Nevertheless, regression-based BIQA models are susceptible to the representativeness and frequency of training samples.

Specifically, the size-limited IQA databases can result in biased training samples, compromising the accuracy of modeling the true distribution of image qualities. Moreover, the regression-based models are derived by minimizing the average prediction error of all training samples, with emphasis on frequent ones. These factors may contribute to a biased estimation of the model parameters [6], causing inaccurate prediction. As shown in Figure 1 (a), the vertical and horizontal coordinates represent image quality and features, respectively. For clarity, the features are shown as points in a one-dimensional space and the black curve represents the fitted BIQA model. If the training set has an inadequate representation of the real sample distribution, the model parameters estimated by the regression loss functions can introduce substantial prediction bias for the test samples, such as the red point in the figure. To alleviate this issue, it is important to avoid over-reliance on specific model parameters. A possible solution is to assess the image quality by retrieving similar instances, such as the pink dots, in the feature space.

Ensuring the validity of the feature space is crucial to obtain sufficiently similar instances. However, it may be difficult to achieve this when the feature representations are learned directly from MOS values. Specifically, the principle of visual masking effects [22, 38, 17] highlights the influence of both image content and distortion on the perceptual function of the human visual system (HVS). Never-



Figure 3: Illustrations of quality correlation and precision among similar content images.

theless, the MOS values primarily reflect the level of quality degradation without providing specific information about the content or distortion type. The image pairs exhibit varying image quality even if they have the same content (Figure 2 (a)) or the same distortion (Figure 2 (c)). Conversely, image pairs with different contents (Figure 2 (b)) or different distortions (Figure 2 (d)) may still have comparable image quality. Therefore, BIQA models derived from regressing MOS values may not effectively model content and distortion representations, hindering their ability to mimic the perception function of the HVS.

In this study, we introduce a regression-free BIQA model for image quality assessment. This model is built on the novel insight that images with similar content and distortion have similar perceptual quality. That is, the nearest neighbors in the feature space based on image content and distortion generally have close quality scores. The proposed model retrieves similar instances from a human-annotated IQA database through the use of two classification modules: the semantic-based classification (SC) module and the distortion-based classification (DC) module. The test image is first compared to pristine images with similar content using the SC module. Then, the DC module queries similar instances within the distorted images corresponding to each retrieved pristine image. Finally, the predicted quality score is obtained by aggregating the MOS values of these similar instances. Figure 1 (b) presents the residual (error term) analysis of the proposed method in comparison with the state-of-the-art regression-based BIQA method [32]. The results of both databases [27, 15] indicate that the residuals of the proposed method exhibit random distribution

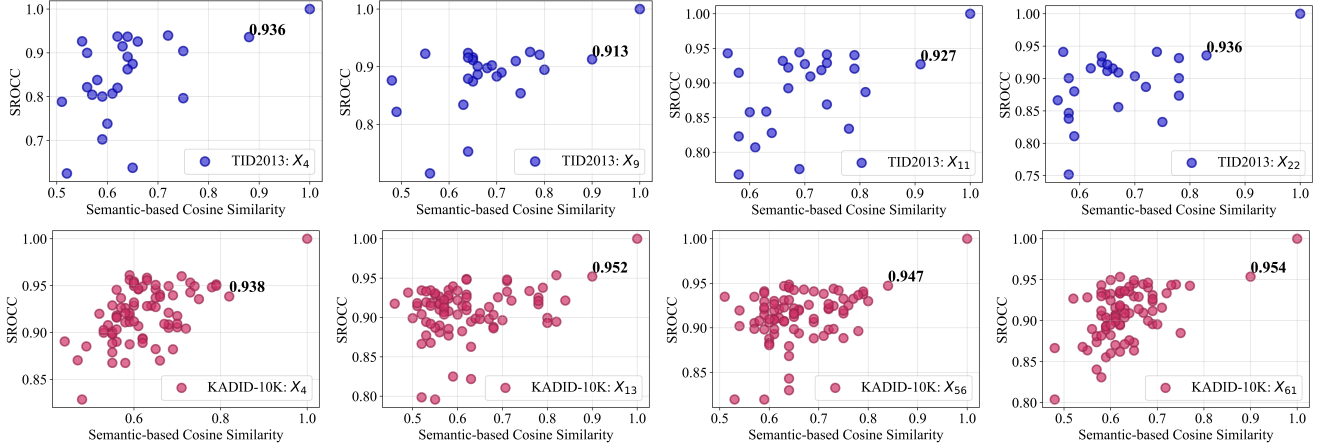


Figure 4: Illustrations of the correlation between the quality of images with similar content and distortion. The notation X_p represents the p -th pristine image of the IQA database.

around zero, providing an evidence for the validity of our model [5, 9].

The main contributions of the paper can be summarized into three aspects: 1) We conduct an analysis of the quality relationship between image content and distortion and arrive at the conclusion that images with similar content demonstrate comparable image quality under the same distortion. 2) We propose a regression-free method to assess image quality by retrieving similar instances in the feature space based on semantic and distortion features. This approach offers nonparametric nature that are effective in reducing prediction bias caused by an unrepresentative training set. 3) We evaluate the proposed model on four benchmark IQA databases and the results demonstrate its significantly superiority over the regression-based BIQA models.

2. Motivation

It has been established that for identical images, the HVS will consistently produce the same visual responses. Additionally, for images with similar content, the HVS will exhibit similar perceptual properties. That is, images with similar content degraded by the same distortion will have comparable visual quality.

As illustrated in Figure 3, pristine image pairs with similar content were obtained from the TID2013 [27] and KADID-10K [15]. The distorted images corresponding to the left image in each pair were used as input for several FR-IQA methods, including SSIM [36], FSIMc [47], and VSI [45]. The evaluation metrics SROCC, PLCC, and RMSE were calculated based on the predicted scores and mean opinion scores (MOS) values. The distorted images corresponding to the right image served as similar instances (SIs) for these input images, with the distortion types and levels aligned. The MOS values of the SIs were taken as the predicted values. The results demonstrate that the SIs

performed best in terms of correlation and precision, indicating that images with similar content generally have similar quality under identical distortions.

To further investigate the quality correlation between images in both content and distortion, semantic feature vectors [8] were calculated for each pristine image to represent its content. The content similarity between two pristine images is determined by the cosine distance between their semantic feature vectors. The correlation between the quality of distorted images associated with these two pristine images was measured using the SROCC of their MOS values, with aligned distortion types and levels. As shown in Figure 4, the quality correlation of distorted images can vary in areas with low semantic similarity, but it tends to be high in regions of high semantic similarity (*e.g.*, greater than 0.8), indicating that images with similar content and distortion have comparable perceptual quality. With this motivation, we devised two classification-based modules, *i.e.*, the SC module and the DC module, which are utilized to identify the content and distortion of an image, respectively. The quality of an image is then determined by retrieving instances that are similar in terms of content and distortion.

3. The proposed Method

3.1. Notations

Given an IQA database, following the sampling protocol for developing IQA models [29, 42, 41, 32], the database is randomly divided into training and test sets, with an 80%-20% split based on pristine images. The training set, consisting of P pristine images, is denoted as $\mathcal{S} = \{(X_p, D_p, M_p) | 1 \leq p \leq P\}$, where X_p denotes the p -th pristine image, $D_p = \{x_p^l | 1 \leq l \leq L\}$ denotes the distorted images corresponding to X_p , with x_p^l denoting the l -th sample in D_p , and M_p denotes the MOS values corresponding to these distorted images.

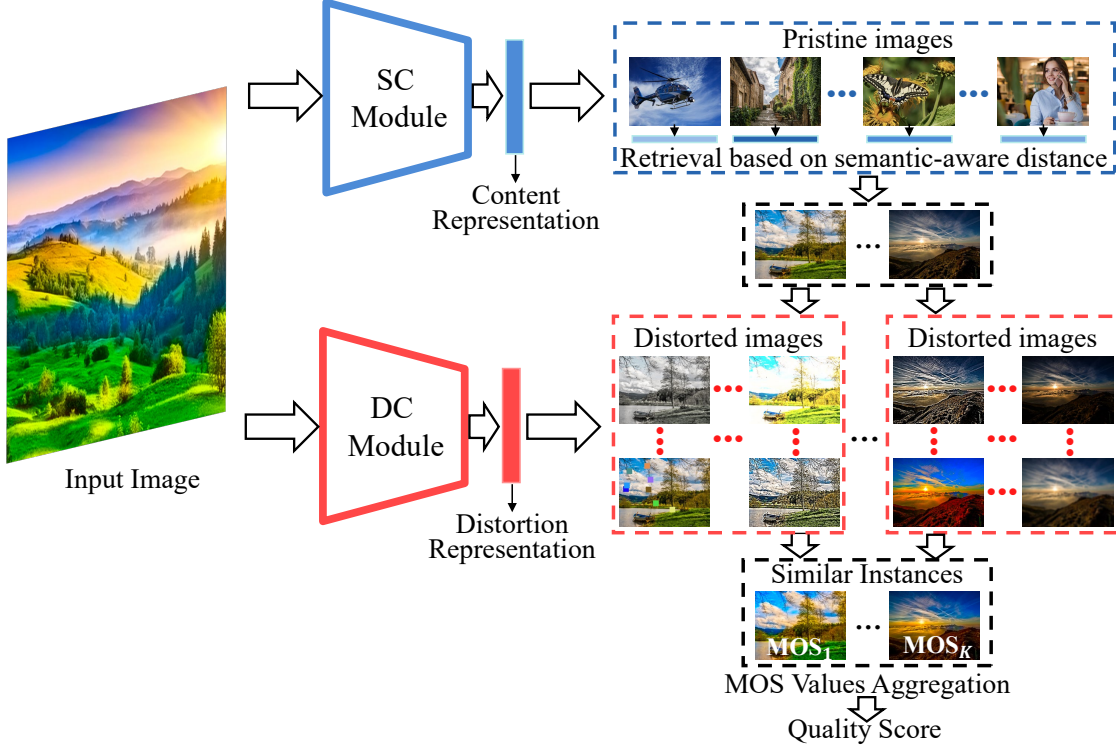


Figure 5: An overview of the proposed model, given an input image and an IQA database. The SC module is utilized to retrieve a pristine image with similar content. Then, the DC module is utilized to retrieve an instance with similar distortion within the distorted images associated with the retrieved pristine image. The final predicted score is obtained by aggregating the MOS values of multiple instances retrieved in this manner.

3.2. Semantic-based Classification (SC) Module

In this subsection, we describe the design of the SC module, which is tasked with extracting the semantic vector to represent image content. Limited the number of pristine images in IQA databases, *e.g.*, TID2013 [27] with only 25 pristine images, the semantic vector distance is used to represent the similarity of image content instead of finding an identical image category. Specifically, the VGG-16 [30] network pre-trained on ImageNet [4] without the last classification layer is taken as the SC module for extracting semantic vectors. Given a test image x_t and a pristine image X_p , the content similarity between x_t and X_p is measured as the semantic-aware distance $\Psi_s(x_t, X_p)$, which is defined as the cosine distance of their semantic feature vectors by

$$\Psi_s(x_t, X_p) = \cos(v_t, v_p) = \frac{v_t \cdot v_p^T}{\|v_t\| \cdot \|v_p\|}, \quad (1)$$

where v_t and v_p denote the semantic vectors of x_t and X_p , respectively. The K pristine images most similar to x_t are retrieved by

$$\left[\hat{X}_p \right]_{p=1}^K = \underset{X_p \in \mathcal{S}}{\operatorname{argsort}_{\mathbb{K}}} \Psi_s(x_t, X_p), \quad (2)$$

where $\operatorname{argsort}_{\mathbb{K}}$ indicates the function sorting the semantic-aware distances in descending order and selecting the first K images, where $1 \leq K \leq P$.

3.3. Distortion-based Classification (DC) Module

In this subsection, we describe the design of the DC module, which is obtained by training a distortion classification model [31] on IQA data. Given a training set with N samples, denoted as $\{(x^n, y^n) \mid 1 \leq n \leq N\}$, where x^n and y^n represent the n -th input image and the ground-truth distortion class indicator vector, respectively. The training objective is to minimize the cross entropy loss function through optimizing the model parameters θ by

$$\hat{\theta} = \underset{\theta}{\operatorname{argmin}} - \sum_{n=1}^N \sum_{c=1}^C y_c^n \log \hat{y}_c^n(x^n; \theta), \quad (3)$$

where C is the number of distortion categories and \hat{y}_c^n represents the predicted probability of the n -th image belonging to the category c . To avoid distortion category bias, the final classification layer of the trained model is removed, and the resulting model is used as the DC module to extract the distortion features. The distortion similarity between the test image x_t and a distorted image x_p^l is calculated as the cosine distance between their distortion feature vectors. This

is represented as the distortion-aware distance $\Psi_d(x_t, x_p^l)$, given by

$$\Psi_d(x_t, x_p^l) = \cos(w_t, w_p^l), \quad (4)$$

where w_t and w_p^l denote the distortion feature vectors of x_t and x_p^l , respectively. Given a pristine image \hat{X}_p retrieved by the SC module, the distorted image with the highest distortion similarity to x_t is retrieved from the set of distorted images D_p , as represented by:

$$\hat{x}_p^l = \operatorname{argmax}_{x_p^l \in D_p} \Psi_d(x_t, x_p^l), \quad (5)$$

The resulting distorted image \hat{x}_p^l is taken as the instance that has a similar perception to x_t in both content and distortion. In this way, multiple instances are retrieved to evaluate the final image quality score.

3.4. Image Quality Prediction

Aggregating the MOS values of multiple retrieved instances can mitigate prediction bias, as a single instance may not be representative of the image being evaluated in all cases. We propose two alternative quality aggregation strategies, *i.e.*, simple average and semantic-aware distance-based weighted average, to evaluate the image quality score. **Simple average.** For the K pristine images retrieved by the SC module, an instance can be obtained for each pristine image by Equation 5. Then, the predicted score of x_t is measured by simply averaging the MOS values of the retrieved instances, which is expressed as

$$\mathcal{Q}_{sim} = \frac{1}{K} \sum_{p=1}^K M_p [\hat{x}_p^l], \quad (6)$$

where $M_p [\hat{x}_p^l]$ represents the ground truth MOS value of the image \hat{x}_p^l .

Semantic-aware distance-based weighted average. The weighted average approach considers the relative impact of each instance on the final quality prediction. Since images with higher semantic similarity tend to exhibit similar perceptual quality under similar distortions, the semantic-aware distance $\Psi_s(x_t, X_p)$ employed as a weighting factor in the averaging of the MOS values, making instances with higher semantic similarity have a greater influence on the final prediction. The predicted quality score can be expressed as

$$\mathcal{Q}_{wei} = \sum_{p=1}^K \frac{\Psi_s(x_t, X_p)}{\sum_p \Psi_s(x_t, X_p)} M_p [\hat{x}_p^l] \quad (7)$$

4. Experimental Results

4.1. Databases

The proposed model is evaluated using four benchmark IQA databases, namely CSIQ [12], TID2013 [27], KADID-10K [15] and LIVE-MD [10]. The images in LIVE-MD are

Table 1: The benchmark databases for BIQA model evaluation.

Database	# of Ref. Images	# of Dist. Types	# of Dist. Images	Score Type
CSIQ [12]	30	6	866	DMOS
TID2013 [27]	25	24	3,000	MOS
KADID-10K [15]	81	25	10,125	MOS
LIVE-MD [10]	15	2	150	DMOS

degraded by multiple distortions, while the images in the other databases are degraded by a single type of distortion. The characteristics of these databases, including the number of pristine images, distortion types, distorted images, and label types, are outlined in Table 1.

4.2. Evaluation criteria

The performance of BIQA models is commonly evaluated using two correlation criteria, namely Spearman’s rank order correlation coefficient (SROCC) and Pearson’s linear correlation coefficient (PLCC). The SROCC measures the monotonic relationship between the ground truth and predicted scores, represented as:

$$\text{SROCC} = 1 - \frac{6 \sum_{i=1}^M d_i^2}{M(M^2 - 1)}, \quad (8)$$

where M is the number of testing images, and d_i is the rank difference between the predicted score and the ground truth value. The PLCC, on the other hand, measures the linear correlation between the ground truth and predicted scores, expressed as:

$$\text{PLCC} = \frac{\sum_{i=1}^M (q_i - u_{q_i})(\hat{q}_i - u_{\hat{q}_i})}{\sqrt{\sum_{i=1}^M (q_i - u_{q_i})^2} \sqrt{\sum_{i=1}^M (\hat{q}_i - u_{\hat{q}_i})^2}}, \quad (9)$$

where q_i and \hat{q}_i denote the ground truth and the predicted score of the i -th image, respectively, and u_{q_i} and $u_{\hat{q}_i}$ are the corresponding mean values, represented as $u_{q_i} = \sum_{i=1}^M q_i$ and $u_{\hat{q}_i} = \sum_{i=1}^M \hat{q}_i$, respectively.

4.3. Implementation details

We leveraged PyTorch [26] as the codebase to implement the proposed model. A classification model [31] was employed to develop the DC module, while due to the limited scale of existing IQA databases as depicted in Table 1, the classification precision was challenging to converge effectively through training solely on IQA databases. To improve the distortion perception of the model, a pre-training phase was conducted, where 40,000 pristine images randomly selected from KADIS-700K [15] were utilized to synthesize numerous distorted images with 30 distortion types, each at five levels. Among these distortion types, 25 were consistent with KADID-10K [15], and the remaining types were over-exposure, under-exposure, contrast change, lossy compression, and pink noise. This experiment was conducted

Table 2: SROCC evaluations on the individual distortions of TID2013. The number of times (N.T) each method achieves the best performance and the average performance are listed in the last two columns.

Method	AGN	ANC	SCN	MN	HFN	IN	QN	GB	DEN	JPEG	JP2K	JGTE	J2TE
HIQA [16]	0.923	0.880	0.945	0.673	0.955	0.810	0.855	0.832	0.957	0.914	0.624	0.460	0.782
DB-CNN[48]	0.790	0.700	0.826	0.646	0.879	0.708	0.825	0.859	0.865	0.894	0.916	0.772	0.773
HyperIQA [32]	0.803	0.503	0.980	0.231	0.857	0.775	0.877	0.777	0.843	0.863	0.900	0.789	0.843
TReS [7]	0.911	0.858	0.938	0.620	0.875	0.701	0.878	0.880	0.883	0.840	0.941	0.753	0.884
CLRIQA [25]	0.816	0.720	0.860	0.395	0.912	0.898	0.879	0.892	0.866	0.940	0.894	0.785	0.865
Ours	0.936	0.812	0.915	0.846	0.942	0.902	0.964	0.915	0.925	0.921	0.914	0.813	0.750
Methods	NEPN	Block	MS	CTC	CCS	MGN	CN	LCNI	ICQD	CHA	SSR	N.T	Average
HIQA [16]	0.664	0.122	0.182	0.376	0.156	0.850	0.614	0.852	0.911	0.381	0.616	4	0.681
DB-CNN[48]	0.270	0.444	-0.009	0.548	0.631	0.711	0.752	0.860	0.833	0.732	0.902	0	0.714
HyperIQA [32]	0.295	0.155	0.228	0.705	0.559	0.874	0.815	0.902	0.820	0.865	0.923	1	0.716
TReS [7]	0.358	0.688	0.344	0.753	0.735	0.815	0.729	0.890	0.805	0.798	0.947	3	0.784
CLRIQA [25]	0.764	0.697	0.387	0.784	0.710	0.801	0.849	0.901	0.894	0.903	0.919	4	0.806
Ours	0.664	0.487	0.514	0.862	0.698	0.918	0.942	0.965	0.899	0.818	0.968	12	0.845

Table 3: Comparison with the state-of-the-art BIQA methods on four benchmark databases.

SROCC \uparrow	CSIQ	TID2013	KADID-10K	LIVE-MD
CORNIA [42]	0.714	0.549	-	0.899
BRISQUE [23]	0.775	0.573	0.450	0.886
ILNIQE [46]	0.821	0.521	0.534	0.902
BIECON [11]	0.815	0.717	0.623	0.912
MEON [21]	0.852	0.808	0.604	0.924
MetalQA[50]	0.899	0.856	0.726	-
CLRIQA [25]	0.915	0.837	0.837	-
DB-CNN [48]	0.946	0.816	0.851	0.927
HyperIQA [32]	0.923	0.840	0.852	0.918
TReS [7]	0.922	0.863	0.859	0.950
Ours	0.957	0.907	0.945	0.930
PLCC \uparrow	CSIQ	TID2013	KADID-10K	LIVE-MD
CORNIA [42]	0.781	0.613	-	0.921
BRISQUE [23]	0.817	0.651	0.482	0.917
ILNIQE [46]	0.865	0.648	0.585	0.914
BIECON [11]	0.823	0.762	0.648	0.928
MEON [21]	0.864	0.824	0.691	0.940
MetalQA[50]	0.908	0.868	0.775	-
CLRIQA [25]	0.938	0.863	0.843	-
DB-CNN [48]	0.959	0.865	0.856	0.934
HyperIQA [32]	0.942	0.858	0.845	0.929
TReS [7]	0.942	0.883	0.858	0.931
Ours	0.960	0.912	0.946	0.943

on NVIDIA Tesla A100 GPUs. Stochastic gradient descent (SGD) with a momentum of 0.9 is adopted to train the model with 40 epochs, with an initial learning rate of 0.05, adjusted by a cosine learning rate scheduler [19]. The mini-batch size is set to 320. Considering the sensitivity of HVS to luminance distortion, each training image is converted to a YCbCr image [1] and rescaled to a size of 288×384 as input.

The experiments were carried out using an NVIDIA RTX 3090 GPU on IQA benchmark databases. The pre-trained distortion classification model was fine-tuned for 30 epochs using the SGD optimizer, with a mini-batch size of 16 and an initial learning rate of $5e-3$. The learning rate was reduced by a factor of 0.5 after every eight epochs. The trained distortion classification model without the fi-

nal linear layer is adopted as the DC module. The VGG-16 pre-trained in ImageNet without the classification layer is adopted as the SC module. The parameter K was set to 9 as the default value for all databases, unless otherwise stated. In the image quality evaluation process, the test image was first fed directly to the SC module, and then randomly cropped to a size of 288×384 before being input to the DC module. To eliminate content overlap, two subsets of pristine images were randomly divided in an 80%-20% ratio to form the training and test sets. The corresponding distorted images were then allocated accordingly. To avoid performance bias, the experiments were conducted 15 times, with random operations, and the median of SROCC and PLCC results were reported. Notably, the training set was only used for training the DC module and retrieving instances, not for quality regression.

4.4. Comparison with the State-of-the-art Methods

Evaluation on individual databases. To assess the performance of the proposed model, experiments were carried out on four IQA databases and the results were compared with ten state-of-the-art BIQA methods, including three traditional methods [46, 42, 23] and seven deep learning-based methods [21, 11, 50, 25, 48, 32, 7]. For the traditional BIQA methods, the results are reproduced by the source code released by the authors. For the deep learning-based methods, the results of the corresponding database are sourced from the original publication or reference [7], while the results of the remaining database are reproduced from the published source code.

As shown in Table 3, the proposed method demonstrates state-of-the-art performance on four benchmark databases. For the two small-scale databases CSIQ and LIVE-MD, the proposed model slightly outperforms the BIQA competitors. However, when tested on larger databases, *i.e.*, TID2013 and KADAD-10K, the proposed method demon-

Table 4: SROCC evaluations on the individual distortions of KADID-10K.

Method	GB	LB	MB	CD	CS	ICQD	CCS	CCS-Lab	JP2K	JPEG	AGN	ANC	IN
HyperIQA [32]	0.902	0.925	0.894	0.905	0.832	0.739	0.511	0.877	0.846	0.819	0.765	0.810	0.833
TReS [7]	0.923	0.938	0.926	0.908	0.889	0.747	0.543	0.858	0.867	0.863	0.792	0.836	0.846
Ours	0.967	0.925	0.974	0.892	0.687	0.810	0.647	0.902	0.934	0.935	0.895	0.939	0.891
Method	MGN	DEN	Brighten	Darken	MS	Jitter	NEPN	Pixelate	QN	Block	HS	CTC	Average
HyperIQA [32]	0.860	0.928	0.811	0.622	0.317	0.882	0.473	0.803	0.723	0.368	0.919	0.333	0.748
TReS [7]	0.883	0.912	0.805	0.628	0.396	0.896	0.385	0.692	0.674	0.574	0.879	0.408	0.763
Ours	0.904	0.924	0.942	0.907	0.696	0.957	0.595	0.847	0.598	0.522	0.921	0.810	0.841

Table 5: Ablation results on different distance metrics.

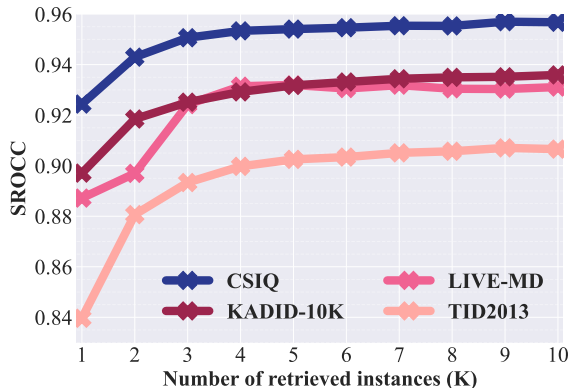
Distance	CSIQ		TID2013	
	SROCC	PLCC	SROCC	PLCC
Euclidean	0.9556	0.9589	0.8961	0.9095
Manhattan	0.9574	0.9587	0.9029	0.9103
Cosine	0.9570	0.9596	0.9071	0.9122

Table 6: Ablation results on different aggregation strategies.

Avg	Number (K)	LIVE-MD		TID2013	
		SROCC	PLCC	SROCC	PLCC
Simple Avg	6	0.9276	0.9379	0.9019	0.9069
	9	0.9259	0.9353	0.9046	0.9077
	10	0.9198	0.9343	0.9065	0.9091
Weighted Avg	6	0.9305	0.9448	0.9035	0.9074
	9	0.9303	0.9427	0.9071	0.9122
	10	0.9311	0.9412	0.9070	0.9097

strates a marked superiority over regression-based methods in terms of both SROCC and PLCC. The reason for this is two-fold. Firstly, increasing the size of the dataset generates a larger set of instances for prediction, leading to improved predictive accuracy of our model. Secondly, as the sample size grows, the regression models need to consider more prediction errors to obtain the overall optimal model. This can, in turn, lead to greater uncertainty in individual predictions. In contrast, our approach retrieves the most similar instances for each sample independently, which makes its superiority more evident in larger databases.

Evaluation on individual distortions. The robustness of the proposed model to distortion has been demonstrated through its performance on individual distortion types of TID2013 and KADID-10K as shown in Table 2 and Table 4, respectively. The results indicate the proposed model surpasses the second-best model by an average SROCC of 4.8%, and demonstrates exceptional performance on 12 out of 24 distortion types. Similarly, in Table 4, the proposed model achieves the best average performance on the KADID-10K database with a margin of 10.2% over the second-best model. These results confirm the robustness of the proposed method to different distortion types.

Figure 6: The impact of different numbers of retrieved instances (*i.e.*, parameter K) on the model performance.

4.5. Ablation study

Distance metrics. As shown in Table 5, various distance metrics were considered as the measures of semantic-aware and distortion-aware distances, including Euclidean, Manhattan, and cosine distance. The results show only slight variations in performance, indicating the robustness of the proposed instance retrieval-based method to different distance metrics.

Number of retrieved instances. As shown in Figure 6, the impact of the number of retrieved instances (*i.e.*, parameter K) on the performance was analyzed. The results indicate that performance improves with an increasing number of instances, especially for K less than 5. However, when K exceeds 5, the performance improvement becomes minimal. The reason for this is that a small number of retrieved instances may introduce prediction bias, which can be reduced by increasing the number of instances. Despite this, it should be noted that our model does not require a large number of instances for accurate image quality evaluation.

Quality aggregation strategies. As shown in Table 6, the results of the ablation experiments demonstrate a comparison between different quality aggregation strategies, including the simple average and the semantic-aware distance-based weighted average. The table demonstrates that, although the weighted average strategy exhibits slightly better performance compared to the simple average, the ma-

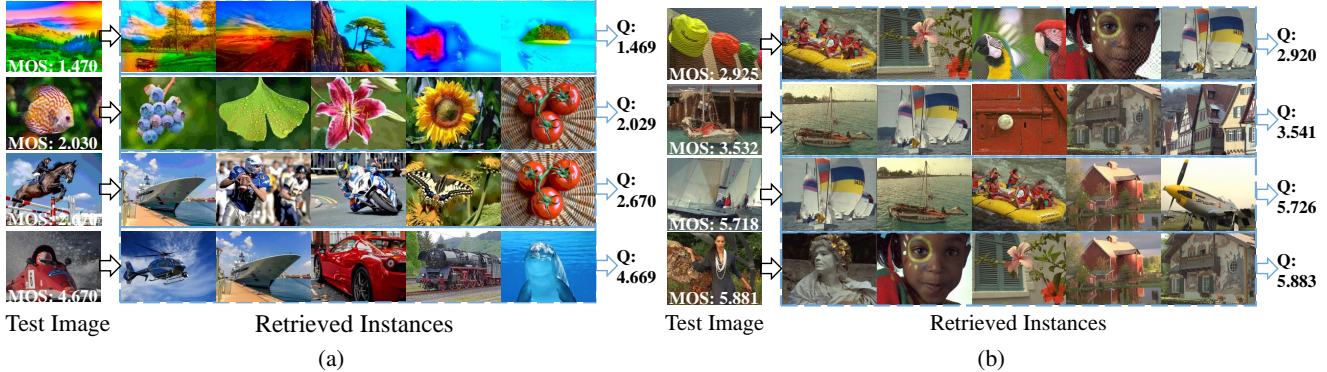


Figure 7: Illustrations of the retrieved results of the proposed model.

Table 7: Ablation results on different image color spaces.

Color Space	CSIQ		TID2013	
	SROCC	PLCC	SROCC	PLCC
RGB	0.9516	0.9518	0.9026	0.9079
YCbCr	0.9570	0.9596	0.9071	0.9122

Table 8: Ablation results on different semantic models.

SC Module	CSIQ		TID2013	
	SROCC	PLCC	SROCC	PLCC
VGG-16 [30]	0.9570	0.9596	0.9071	0.9122
VGG-19 [30]	0.9576	0.9595	0.9057	0.9144
ResNet-18 [8]	0.9599	0.9570	0.9008	0.9138
ResNet-34 [8]	0.9588	0.9566	0.9016	0.9149
ResNet-50 [8]	0.9584	0.9553	0.9024	0.9148
EfficientNet-B0 [33]	0.9563	0.9570	0.8995	0.8848
EfficientNet-B5 [33]	0.9557	0.9570	0.9030	0.8782

majority of the improvement in the model performance can be attributed to the effective instance retrieval scheme.

Image color space for DC module. As shown in Table 7, utilizing the YCbCr image as the input for the DC module results in improved performance compared to the use of the RGB image. This improvement can be attributed to the fact that the YCbCr image separates the information on luminance and chrominance, allowing the model to independently identify distortions in each of these components.

Semantic models for SC module. As shown in Table 8, the results of the ablation studies demonstrate the impact of different semantic-based models employed as the SC module. Despite variations in the number of parameters and classification accuracy on the ImageNet, all models demonstrate comparable performance, highlighting the independence of the proposed model from the precision of semantic representations generated by the SC module. This enhances the generalizability and flexibility of the proposed BIQA model.

5. Discussion

Analysis of model complexity. Considering the requirements of practical application scenarios, such as model complexity and processing time, the proposed model stores

Table 9: Complexity analysis of the proposed model.

Database	Size	Time	SROCC	PLCC
CSIQ	0.25M ($dim=32$)	16.66ms	0.9066	0.9131
	0.49M ($dim=64$)	16.59ms	0.9319	0.9349
	0.99M ($dim=128$)	16.63ms	0.9487	0.9534
	1.97M ($dim=256$)	16.80ms	0.9534	0.9656
	3.94M ($dim=512$)	18.33ms	0.9548	0.9561
TID2013	0.84M ($dim=32$)	17.21ms	0.8566	0.8607
	1.66M ($dim=64$)	17.37ms	0.8725	0.8856
	3.33M ($dim=128$)	17.39ms	0.8865	0.8958
	6.65M ($dim=256$)	17.11ms	0.8990	0.9044
	13.30M ($dim=512$)	19.37ms	0.9033	0.9067

only the feature vectors and corresponding MOS values of the retrieved images. To reduce storage space, 1D max pooling is applied to these feature vectors, resulting in lower dimensions such as 512, 256, or 128. As demonstrated in Table 9, the reduced-dimensional features require minimal storage space with a slight impact on performance. For instance, the CSIQ and TID2013 databases require 1.97M and 6.65M, respectively, with little performance degradation when using 256-dimensional features. Additionally, when evaluating 1000 images using an NVIDIA RTX 3090 GPU with a batch size of 1, the average processing time per image is below 20 ms.

Analysis of retrieval results. We present a visualization of the retrieved instances of our proposed model in Figures 7 (a) and (b). These figures demonstrate the capability of our model to retrieve instances with similar content and distortion as the test images. For instance, as shown in the top row of Figure 7 (a), our model is able to identify landscape pictures with severe color distortion that are similar to the test image. Moreover, the model can effectively detect similarities in contours and colors, as demonstrated in the bottom row of Figure 7 (a), where the retrieved instances display similarity in both contours (e.g., the helicopter and the ship) and color (e.g., the red car). These results demonstrate the effectiveness of our model in perceiving image content and distortion and evaluating image quality through the retrieval of similar perceptual instances.

6. Conclusion

The existing regression-based BIQA models suffer from the presence of biased training samples. This issue can lead to a biased estimation of the model parameters, thereby affecting its predictive ability. In this work, we present a novel regression-free approach for image quality assessment, which consists of two classification modules, namely the SC module and the DC module. The proposed model evaluates the quality of an input image by retrieving instances from a database with similar image content and distortion. Our method establishes local relationships between neighboring instances in the feature space, rather than relying on the entire training set as in regression methods. This allows the proposed model to effectively reduce the prediction bias caused by a biased training set, by avoiding over-reliance on specific model parameters. The superiority of the proposed method is demonstrated by the experimental results on four benchmark IQA databases.

References

- [1] RECOMMENDATION ITU-R BT et al. Studio encoding parameters of digital television for standard 4: 3 and wide-screen 16: 9 aspect ratios. *Int. Radio Consultative Committee Int. Telecommun. Union, Switzerland, CCIR Rep*, pages 624–4, 2011. 6
- [2] Yoojin Choi, Mostafa El-Khamy, and Jungwon Lee. Variable rate deep image compression with a conditional autoencoder. In *Proceedings of the IEEE/CVF International Conference on Computer Vision (ICCV)*, October 2019. 1
- [3] Li Sze Chow and Raveendran Paramesran. Review of medical image quality assessment. *Biomedical signal processing and control*, 27:145–154, 2016. 1
- [4] Jia Deng, Wei Dong, Richard Socher, Li-Jia Li, Kai Li, and Li Fei-Fei. Imagenet: A large-scale hierarchical image database. In *2009 IEEE Conference on Computer Vision and Pattern Recognition*, pages 248–255, 2009. 4
- [5] Andy Field. *Discovering statistics using IBM SPSS statistics*. sage, 2013. 3
- [6] Andrew Gelman and Jennifer Hill. *Data analysis using regression and multilevel/hierarchical models*. Cambridge university press, 2006. 2
- [7] S Alireza Golestaneh, Saba Dadsetan, and Kris M Kitani. No-reference image quality assessment via transformers, relative ranking, and self-consistency. In *Proceedings of the IEEE/CVF Winter Conference on Applications of Computer Vision*, pages 3209–3218, 2022. 2, 6, 7
- [8] Kaiming He, Xiangyu Zhang, Shaoqing Ren, and Jian Sun. Deep residual learning for image recognition. In *2016 IEEE Conference on Computer Vision and Pattern Recognition (CVPR)*, pages 770–778, 2016. 3, 8
- [9] Gareth James, Daniela Witten, Trevor Hastie, and Robert Tibshirani. *An introduction to statistical learning*, volume 112. Springer, 2013. 3
- [10] Dinesh Jayaraman, Anish Mittal, Anush K. Moorthy, and Alan C. Bovik. Objective quality assessment of multiply distorted images. In *2012 Conference Record of the Forty Sixth Asilomar Conference on Signals, Systems and Computers (ASILOMAR)*, pages 1693–1697, 2012. 1, 5
- [11] Jongyoo Kim and Sanghoon Lee. Fully deep blind image quality predictor. *IEEE Journal of Selected Topics in Signal Processing*, 11(1):206–220, 2017. 2, 6
- [12] Eric Cooper Larson and Damon Michael Chandler. Most apparent distortion: full-reference image quality assessment and the role of strategy. *Journal of electronic imaging*, 19(1):011006, 2010. 1, 5
- [13] Qiaohong Li, Weisi Lin, Jingtao Xu, and Yuming Fang. Blind image quality assessment using statistical structural and luminance features. *IEEE Transactions on Multimedia*, 18(12):2457–2469, 2016. 1
- [14] Jingyun Liang, Guolei Sun, Kai Zhang, Luc Van Gool, and Radu Timofte. Mutual affine network for spatially variant kernel estimation in blind image super-resolution. In *Proceedings of the IEEE/CVF International Conference on Computer Vision*, pages 4096–4105, 2021. 1
- [15] Hanhe Lin, Vlad Hosu, and Dietmar Saupe. Kadid-10k: A large-scale artificially distorted iqa database. In *2019 Eleventh International Conference on Quality of Multimedia Experience (QoMEX)*, pages 1–3, 2019. 1, 2, 3, 5
- [16] Kwan-Yee Lin and Guanxiang Wang. Hallucinated-iqa: No-reference image quality assessment via adversarial learning. In *2018 IEEE/CVF Conference on Computer Vision and Pattern Recognition*, pages 732–741, 2018. 6
- [17] Weisi Lin and Gheorghita Ghinea. Progress and opportunities in modelling just-noticeable difference (jnd) for multimedia. *IEEE Transactions on Multimedia*, pages 1–1, 2021. 2
- [18] Xialei Liu, Joost Van De Weijer, and Andrew D. Bagdanov. Rankiqa: Learning from rankings for no-reference image quality assessment. In *2017 IEEE International Conference on Computer Vision (ICCV)*, pages 1040–1049, 2017. 2
- [19] Ilya Loshchilov and Frank Hutter. Sgdr: Stochastic gradient descent with warm restarts. *arXiv preprint arXiv:1608.03983*, 2016. 6
- [20] Guo Lu, Tianxiong Zhong, Jing Geng, Qiang Hu, and Dong Xu. Learning based multi-modality image and video compression. In *2022 IEEE/CVF Conference on Computer Vision and Pattern Recognition (CVPR)*, pages 6073–6082, 2022. 1
- [21] Kede Ma, Wentao Liu, Kai Zhang, Zhengfang Duanmu, Zhou Wang, and Wangmeng Zuo. End-to-end blind image quality assessment using deep neural networks. *IEEE Transactions on Image Processing*, 27(3):1202–1213, 2018. 2, 6
- [22] Stephen L Macknik and Margaret S Livingstone. Neuronal correlates of visibility and invisibility in the primate visual system. *Nature neuroscience*, 1(2):144–149, 1998. 2
- [23] Anish Mittal, Anush Krishna Moorthy, and Alan Conrad Bovik. No-reference image quality assessment in the spatial domain. *IEEE Transactions on Image Processing*, 21(12):4695–4708, 2012. 1, 6
- [24] Anush Krishna Moorthy and Alan Conrad Bovik. Blind image quality assessment: From natural scene statistics to perceptual quality. *IEEE Transactions on Image Processing*, 20(12):3350–3364, 2011. 1

- [25] Fu-Zhao Ou, Yuan-Gen Wang, Jin Li, Guopu Zhu, and Sam Kwong. A novel rank learning based no-reference image quality assessment method. *IEEE Transactions on Multimedia*, pages 1–1, 2021. 2, 6
- [26] Adam Paszke, Sam Gross, Francisco Massa, Adam Lerer, James Bradbury, Gregory Chanan, Trevor Killeen, Zeming Lin, Natalia Gimelshein, Luca Antiga, et al. Pytorch: An imperative style, high-performance deep learning library. *Advances in neural information processing systems*, 32, 2019. 5
- [27] Nikolay Ponomarenko, Lina Jin, Oleg Ieremeiev, Vladimir Lukin, Karen Egiazarian, Jaakko Astola, Benoit Vozel, Kacem Chehdi, Marco Carli, Federica Battisti, et al. Image database tid2013: Peculiarities, results and perspectives. *Signal processing: Image communication*, 30:57–77, 2015. 1, 2, 3, 4, 5
- [28] Kuldeep Purohit, Maitreya Suin, AN Rajagopalan, and Vishnu Naresh Boddeti. Spatially-adaptive image restoration using distortion-guided networks. In *Proceedings of the IEEE/CVF International Conference on Computer Vision*, pages 2309–2319, 2021. 1
- [29] Michele A. Saad, Alan C. Bovik, and Christophe Charrier. Blind image quality assessment: A natural scene statistics approach in the dct domain. *IEEE Transactions on Image Processing*, 21(8):3339–3352, 2012. 1, 3
- [30] Karen Simonyan and Andrew Zisserman. Very deep convolutional networks for large-scale image recognition. In *International Conference on Learning Representations*, 2015. 4, 8
- [31] Aravind Srinivas, Tsung-Yi Lin, Niki Parmar, Jonathon Shlens, Pieter Abbeel, and Ashish Vaswani. Bottleneck transformers for visual recognition. In *2021 IEEE/CVF Conference on Computer Vision and Pattern Recognition (CVPR)*, pages 16514–16524, 2021. 4, 5
- [32] Shaolin Su, Qingsen Yan, Yu Zhu, Cheng Zhang, Xin Ge, Jinqiu Sun, and Yanning Zhang. Blindly assess image quality in the wild guided by a self-adaptive hyper network. In *2020 IEEE/CVF Conference on Computer Vision and Pattern Recognition (CVPR)*, pages 3664–3673, 2020. 2, 3, 6, 7
- [33] Mingxing Tan and Quoc Le. Efficientnet: Rethinking model scaling for convolutional neural networks. In *International conference on machine learning*, pages 6105–6114. PMLR, 2019. 8
- [34] Domonkos Varga, Dietmar Saupe, and Tamás Szirányi. Deepnrn: A content preserving deep architecture for blind image quality assessment. In *2018 IEEE International Conference on Multimedia and Expo (ICME)*, pages 1–6, 2018. 2
- [35] Wei Wang, Ruiming Guo, Yapeng Tian, and Wenming Yang. Cfsnet: Toward a controllable feature space for image restoration. In *Proceedings of the IEEE/CVF International Conference on Computer Vision (ICCV)*, October 2019. 1
- [36] Zhou Wang, A.C. Bovik, H.R. Sheikh, and E.P. Simoncelli. Image quality assessment: from error visibility to structural similarity. *IEEE Transactions on Image Processing*, 13(4):600–612, 2004. 3
- [37] Zhou Wang and Alan C Bovik. Modern image quality assessment. *Synthesis Lectures on Image, Video, and Multimedia Processing*, 2(1):1–156, 2006. 1
- [38] Jinjian Wu, Leida Li, Weisheng Dong, Guangming Shi, Weisi Lin, and C.-C. Jay Kuo. Enhanced just noticeable difference model for images with pattern complexity. *IEEE Transactions on Image Processing*, 26(6):2682–2693, 2017. 2
- [39] Jingtao Xu, Peng Ye, Qiaohong Li, Haiqing Du, Yong Liu, and David Doermann. Blind image quality assessment based on high order statistics aggregation. *IEEE Transactions on Image Processing*, 25(9):4444–4457, 2016. 1
- [40] Wufeng Xue, Lei Zhang, and Xuanqin Mou. Learning without human scores for blind image quality assessment. In *Proceedings of the IEEE Conference on Computer Vision and Pattern Recognition (CVPR)*, June 2013. 1
- [41] Sheng Yang, Qiuping Jiang, Weisi Lin, and Yongtao Wang. Sgdnet: An end-to-end saliency-guided deep neural network for no-reference image quality assessment. In *Proceedings of the 27th ACM International Conference on Multimedia*, pages 1383–1391, 2019. 2, 3
- [42] Peng Ye, Jayant Kumar, Le Kang, and David Doermann. Un-supervised feature learning framework for no-reference image quality assessment. In *2012 IEEE Conference on Computer Vision and Pattern Recognition*, pages 1098–1105, 2012. 1, 3, 6
- [43] Junyong You and Jari Korhonen. Transformer for image quality assessment. In *2021 IEEE International Conference on Image Processing (ICIP)*, pages 1389–1393, 2021. 2
- [44] Fei Yuan, Yifan Huang, Xin Chen, and En Cheng. A biological sensor system using computer vision for water quality monitoring. *IEEE Access*, 6:61535–61546, 2018. 1
- [45] Lin Zhang, Ying Shen, and Hongyu Li. Vsi: A visual saliency-induced index for perceptual image quality assessment. *IEEE Transactions on Image Processing*, 23(10):4270–4281, 2014. 3
- [46] Lin Zhang, Lei Zhang, and Alan C. Bovik. A feature-enriched completely blind image quality evaluator. *IEEE Transactions on Image Processing*, 24(8):2579–2591, 2015. 1, 6
- [47] Lin Zhang, Lei Zhang, Xuanqin Mou, and David Zhang. Fsim: A feature similarity index for image quality assessment. *IEEE Transactions on Image Processing*, 20(8):2378–2386, 2011. 3
- [48] Weixia Zhang, Kede Ma, Jia Yan, Dexiang Deng, and Zhou Wang. Blind image quality assessment using a deep bilinear convolutional neural network. *IEEE Transactions on Circuits and Systems for Video Technology*, 30(1):36–47, 2020. 2, 6
- [49] Ruofan Zhou and Sabine Susstrunk. Kernel modeling super-resolution on real low-resolution images. In *Proceedings of the IEEE/CVF International Conference on Computer Vision (ICCV)*, October 2019. 1
- [50] Hancheng Zhu, Leida Li, Jinjian Wu, Weisheng Dong, and Guangming Shi. Metaiqa: Deep meta-learning for no-reference image quality assessment. In *Proceedings of the IEEE/CVF Conference on Computer Vision and Pattern Recognition (CVPR)*, June 2020. 2, 6